Melinda T. Coughlan,[1,2,3] Gavin C. Higgins,[1] Tuong-Vi Nguyen,[1] Sally A. Penfold,[1] Vicki Thallas-Bonke,[1] Sih Min Tan,[1,2] Georg Ramm,[4] Nicole J. Van Bergen,[5] Darren C. Henstridge,[1] Karly C. Sourris,[1,2] Brooke E. Harcourt,[6] Ian A. Trounce,[5] Portia M. Robb,[1] Adrienne Laskowski,[6] Sean L. McGee,[7] Amanda J. Genders,[7] Ken Walder,[7] Brian G. Drew,[1] Paul Gregorevic,[1] Hongwei Qian,[1] Merlin C. Thomas,[1] George Jerums,[8] Richard J. Macisaac,[9] Alison Skene,[10] David A. Power,[11,12] Elif I. Ekinci,[8,12,13] Xiaonan W. Wijeyeratne,[14] Linda A. Gallo,[15] Michal Herman-Edelstein,[16] Michael T. Ryan,[17] Mark E. Cooper,[1,2] David R. Thorburn,[6] and Josephine M. Forbes[1,15,18]

Deficiency in Apoptosis-Inducing Factor Recapitulates Chronic Kidney Disease via Aberrant Mitochondrial Homeostasis

Diabetes 2016;65:1085–1098 | DOI: 10.2337/db15-0864

Apoptosis-inducing factor (AIF) is a mitochondrial flavoprotein with dual roles in redox signaling and programmed cell death. Deficiency in AIF is known to result in defective oxidative phosphorylation (OXPHOS), via loss of complex I activity and assembly in other tissues. Because the kidney relies on OXPHOS for metabolic homeostasis, we hypothesized that a decrease in AIF would result in chronic kidney disease (CKD). Here, we report that partial knockdown of *Aif* in mice recapitulates many features of CKD, in association with a compensatory increase in the mitochondrial ATP pool via a shift toward mitochondrial fusion, excess mitochondrial reactive oxygen species production, and *Nox4* upregulation. However, despite a 50% lower AIF protein content in the kidney cortex, there was no loss of complex I activity or assembly. When diabetes was superimposed onto *Aif* knockdown, there were extensive changes in mitochondrial function and networking, which augmented the renal lesion. Studies in patients with diabetic nephropathy showed a decrease in AIF within the renal tubular compartment and lower *AIFM1* renal cortical gene expression, which correlated with declining glomerular filtration rate. Lentiviral overexpression of *Aif1m* rescued glucose-induced disruption of mitochondrial respiration in human primary proximal tubule cells. These studies demonstrate that AIF deficiency is a risk factor for the development of diabetic kidney disease.

[1]Baker IDI Heart and Diabetes Institute, Melbourne, Victoria, Australia
[2]Department of Medicine, Central Clinical School, Monash University, Alfred Medical Research and Education Precinct, Melbourne, Victoria, Australia
[3]Department of Epidemiology and Preventive Medicine, Monash University, Alfred Medical Research and Education Precinct, Melbourne, Victoria, Australia
[4]Membrane Biology Group, Department of Biochemistry and Molecular Biology, Monash University, Clayton Campus, Victoria, Australia
[5]Centre for Eye Research Australia, Royal Victorian Eye and Ear Hospital, East Melbourne, Victoria, Australia
[6]Murdoch Children's Research Institute, Royal Children's Hospital, Parkville, Victoria, Australia
[7]Metabolic Research Unit, Deakin University, Waurn Ponds, Victoria, Australia
[8]Endocrine Centre, Austin Health, Repatriation Campus, Heidelberg West, Victoria, Australia
[9]Departments of Endocrinology and Diabetes, St Vincent's Hospital Melbourne and The University of Melbourne, Fitzroy, Victoria, Australia
[10]Department of Anatomical Pathology, Austin Health, Heidelberg, Victoria, Australia
[11]Department of Nephrology and Institute for Breathing and Sleep, Austin Health, Heidelberg, Victoria, Australia
[12]Department of Medicine, Austin Health and The University of Melbourne, Parkville, Victoria, Australia
[13]Menzies School of Health Research, Darwin, Northern Territory, Australia
[14]Department of Biochemistry, La Trobe University, Melbourne, Victoria, Australia
[15]Glycation and Diabetes Group, Mater Research Institute-University of Queensland, Translational Research Institute, Woolloongabba, South Brisbane, Queensland, Australia
[16]The Felsenstein Medical Research Center and Department of Nephrology and Hypertension, Rabin Medical Center, Sackler Faculty of Medicine, Tel Aviv University, Tel Aviv, Israel
[17]Mitochondria Laboratory, Department of Biochemistry and Molecular Biology, Monash University, Clayton, Victoria, Australia
[18]School of Medicine, Mater Clinical School, The University of Queensland, St. Lucia, Queensland, Australia

Corresponding author: Melinda T. Coughlan, melinda.coughlan@bakeridi.edu.au.

Received 24 June 2015 and accepted 10 January 2016.

This article contains Supplementary Data online at http://diabetes.diabetesjournals.org/lookup/suppl/doi:10.2337/db15-0864/-/DC1.

Normal kidney function is energetically demanding, and the proximal tubule of the kidney generates vast quantities of ATP via oxidative phosphorylation (OXPHOS) to facilitate active reabsorption of macromolecules such as glucose and lactate, which would otherwise be lost into the urine (1). There is increasing evidence to indicate that the disruption of mitochondrial bioenergetics, which leads to altered capacity for ATP production, may contribute to the development and progression of chronic kidney disease (CKD) (2,3). This includes in the setting of diabetic nephropathy (DN) (4–10), but the specific molecular mechanisms linking mitochondrial dysfunction to CKD remain to be elucidated.

The mitochondrial flavoprotein apoptosis-inducing factor (AIF) was initially discovered as the first caspase-independent cell death effector mediating chromatin condensation and DNA fragmentation (11). However, AIF can promote cell survival independently from its role as a cell death effector, via NADH oxidoreductase and redox activity (12). Previous studies have shown that the Harlequin (Hq; *Aifm1*$^{Hq/Y}$) mouse, which has a loss of AIF protein of up to 80% relative to wild-type (WT) mice (13), has a decrease in complex I activity in a variety of organs (14,15), which is reminiscent of human complex I mitochondrial deficiency syndromes. Other studies (15) have also linked AIF to the stabilization, assembly, and activity of complex I. Given the role for AIF in the regulation of OXPHOS in other tissues, and the vast quantities of ATP required to maintain metabolic homeostasis in the kidney, we hypothesized the following: *1*) that AIF may be important for normal kidney function, *2*) that decreasing AIF would impair kidney function and alter structure, and *3*) that restoring AIF would ameliorate bioenergetic defects. Here, we show that *1*) renal AIF protein and gene expression are significantly decreased in human DN, in proportion to the impairment of renal function (by estimated glomerular filtration rate [eGFR]); *2*) *Aifm1*$^{Hq/Y}$ mice, which have a 50% reduction in AIF within the kidney, exhibit hallmarks of CKD, including proteinuria, glomerulosclerosis, tubulointerstitial fibrosis, and hyperfiltration, in parallel with altered mitochondrial dynamics and bioenergetics; *3*) induction of experimental diabetes in *Aifm1*$^{Hq/Y}$ mice resulted in more severe kidney disease than in WT diabetic mice; and *4*) overexpression of AIF in primary proximal tubule epithelial cells (PTECs) restored OXPHOS capacity following a high glucose insult. These studies indicate a role for AIF in the development of human renal pathologies such as CKD.

RESEARCH DESIGN AND METHODS

Mouse Model

All animal experiments were performed in accordance with guidelines from the Alfred Medical Research and Education Precinct Animal Ethics Committee and the National Health and Medical Research Council of Australia. Four-week-old male mice hemizygous for the Hq mutation (F1 generation) in the *Aifm1* gene, which encodes for AIF and their littermate controls (WT) were purchased from The Jackson Laboratory (Bar Harbor, ME) (B6CBACa*A*$^{w\text{-}J}$/*A-Aifm1*^{Hq}/J; http://jaxmice.jax.org/strain/000501.html). Mice were housed in a temperature-controlled environment, with a 12-h light/dark cycle and access to chow (Specialty Feeds, Perth, WA, Australia) and water ad libitum. Diabetes was induced in 6-week-old mice (n = 15 mice/group, WT D or Hq D) by five daily intraperitoneal injections of low-dose streptozotocin (55 mg/kg; Sigma-Aldrich, St. Louis, MO) as previously described (16). At 10 weeks after the induction of diabetes, mice were placed individually into metabolic cages (Iffa Credo, L'Arbresele, France) for 24 h. Blood glucose levels were measured using a glucometer (Accutrend; Boehringer Manheim Biochemica, Manheim, Germany). Glycated hemoglobin (GHb) was determined using a Cobas Integra 400 Autoanalyzer (Roche Diagnostics Corporation). After 10 weeks, animals were euthanized, and the kidneys were rapidly dissected, weighed, and snap frozen or placed in 10% neutral buffered formalin (v/v) for fixation before paraffin embedding. In a subset of mice (n = 5 per group), mitochondria were isolated from fresh renal cortices, as described later. Renal cortices from three mice per group were processed for transmission electron microscopy, as described below.

Renal Function and Morphometry

Urinary and plasma creatinine concentrations were measured by high-performance liquid chromatography (16). Mouse-specific ELISAs were used to measure urinary albumin excretion (Bethyl Laboratories, Montgomery, TX), urinary kidney injury molecule-1 (KIM-1) (USCN Life Sciences, Wuhan, China), plasma cystatin C (BioVendor, Mordice, Czech Republic), and urinary neutrophil gelatinase–associated lipocalin (NGAL) (R&D Systems, Minneapolis, MN) as per the manufacturer specifications. Glomerulosclerotic index (GSI) was assessed in periodic acid Schiff (PAS)–stained sections, as previously described (17). Tubulointerstitial area was evaluated in PAS-stained sections by point counting, as previously described (16). Immunohistochemistry for collagen IV was performed in paraffin-embedded kidney sections using a goat polyclonal collagen IV antibody as previously described (Southern Biotech, Birmingham, AL) (18).

Electron Microscopy and Analysis of Mitochondrial Morphology

Immediately following exsanguination, renal cortices were fixed in 2.5% glutaraldehyde in 0.1 mol/L sodium cacodylate buffer, and tissue was processed for standard transmission electron microscopy using postfixation in 1% OsO_4 and embedding in EPON resin. Ultrathin sections were cut and stained with lead citrate and uranyl acetate, and were imaged on a Hitachi H-7500 Transmission Electron Microscope equipped with a Gatan MultiScan 791 charged-coupled device camera. Up to 10

images of PTECs per kidney section were randomly collected for each mouse at ×15,000 magnification. Mitochondrial length and width of all mitochondria within a given image (from five to six images per mouse) were measured using ImageJ, and the aspect ratio was calculated (length/width) and expressed as the mean aspect ratio per group. In addition, the number of mitochondria within each field per section was evaluated and expressed as the mean mitochondrial number per group.

Mitochondrial Isolation

Mitochondria from fresh mouse kidneys were isolated from 100 mg of renal cortex by differential centrifugation, as previously described (2).

ATP Content

Mitochondrial ATP was measured using a Molecular Probes bioluminescence ATP determination kit (Life Technologies, Melbourne, VIC, Australia), as described previously (19,20) with the following modifications. A 10-point standard curve was prepared, ranging from 50,000 to 125 nmol/L.

Oxygen Consumption Rate

The oxygen consumption rate (OCR) in isolated mitochondria from the renal cortex of WT and Hq mice was measured using a Clarke electrode, as described elsewhere (21). OCRs in isolated mitochondria from WT diabetic, Hq, and Hq diabetic mice were measured using an Oxygraph-2k high-resolution respirometer (Oroboros Instruments, Innsbruck, Austria) (22). Units were calculated as oxygen consumption in nanograms of atoms of oxygen per minute per milligram of protein, and data were normalized to the percent of WT control.

Mitochondrial Superoxide Production

Superoxide generation in freshly isolated mitochondria was measured using a Molecular Probes MitoSOX Red probe (Thermo Fisher Scientific, Eugene, OR), and fluorescence was measured by flow cytometry as previously described (2).

Superoxide Dismutase Activity

The activity of superoxide dismutase in isolated mitochondria was assayed using an assay kit of Cayman Chemical Company (Ann Arbor, MI) according to the instructions of the manufacturer.

Complex I Activity and Citrate Synthase Activity

Respiratory chain complex I and citrate synthase activity were assayed by standard spectrophotometric methods in renal cortical supernatants as previously described (2).

3-Nitrotyrosine ELISA

3-Nitrotyrosine (3-NT) was measured in mitochondrial isolates (neat) using the BIOXYTECH Nitrotyrosine EIA kit (OxisResearch, Portland, OR), as specified by the manufacturer.

Western Immunoblotting

Renal cortices were homogenized using a Bullet Blender 24 (Next Advance, Averill Park, NY) at 4°C, with 1.00- and 2.00-mm beads at speed 8 for 4 min in radioimmunoprecipitation assay extraction buffer (10 mmol/L Tris-HCl, pH 8.0; 150 mmol/L NaCl; 1% NP-40; 1% sodium deoxycholate; 0.1% SDS), containing Protease Inhibitor Cocktail (Roche, Castle Hill, NSW, Australia) and Phosphatase Inhibitor Cocktail 2 (Sigma-Aldrich [Pty] Ltd., Sydney, NSW, Australia). The supernatant was obtained following centrifugation (15,000*g*, for 15 min) at 4°C, and protein content was determined using a Pierce BCA Protein Assay Kit (Thermo Fisher Scientific, Melbourne, VIC, Australia). Immunoblotting was performed using the following primary antibodies: mouse monoclonal anti-AIF (Clone E-1) antibody (1:1,000; Santa Cruz Biotechnology, Santa Cruz, CA), β-actin (AC-15; 1:10,000) and cyclooxygenase IV (COX IV; 1:10,000) antibodies (Abcam, Melbourne, VIC, Australia), mouse monoclonal anti–optic atrophy 1 (OPA1) and dynamin-related protein 1 (Drp-1) antibodies (1:1,000; BD Transduction Laboratories, North Ryde, NSW, Australia), rabbit anti–mitofusin (MFN)-1 (Abcam), and rabbit anti-MFN2 (Cell Signaling Technology).

Blue Native PAGE

Mitochondria (40 μg protein), obtained as described in the above section, were solubilized in 50 μL 1% (w/v) digitonin (Calbiochem) or 1% (w/v) Triton X-100 (Sigma-Aldrich) in 50 mmol/L NaCl; 20 mmol/L Bis-Tris, pH 7.0; and 10% (w/v) glycerol, and subjected to a 4–10% gradient blue native PAGE (23).

Quantitative RT-PCR

RNA was isolated from kidney cortex (20–30 mg) or human primary PTECs using TRIzol Reagent (Life Technologies) as previously described. DNA-free RNA was reverse transcribed into cDNA using the SuperScript First Strand Synthesis System according to the manufacturer specifications (Life Technologies BRL, Grand Island, NY). Real-time PCR was performed using either TaqMan assays or SYBR green PCR mix (primer concentration of 500 nmol/L; Applied Biosystems, Mulgrave, VIC, Australia) using a 7500 Fast Real-time PCR System (Applied Biosystems), and normalized relative to the 18*S* ribosomal RNA. For TaqMan reactions, the relative fold difference in expression was calculated using the comparative $2^{-\Delta\Delta Ct}$ method. Primers and probes were designed with Primer Express 2.0 software (Applied Biosystems). The nucleotide sequences for primers and probes examined are shown in Supplementary Table 1.

Human PTEC Culture

Human primary PTECs obtained from American Type Culture Collection (ATCC) (Manassas, VA) were maintained in Renal Epithelial Cell Basal Medium (ATCC) supplemented with the Renal Epithelial Cell Growth Kit (ATCC). PTECs, at 80% confluency, were exposed to normal

glucose (5 mmol/L D-glucose), high glucose (25 mmol/L D-glucose), or osmotic control (5 mmol/L D-glucose and 20 mmol/L mannitol) for 48 h, after which RNA was extracted and *Aifm1* (encoding AIF) expression was measured by quantitative PCR (qPCR). In subsequent cell culture experiments, AIF was overexpressed in human primary PTECs using lentiviral vectors as described below.

Construction and Generation of Lentiviral Vectors

The mouse AIF vector (cFugw-AIF-GFP) was a gift from Drs. Ted and Valina Dawson from The Johns Hopkins University School of Medicine (Baltimore, MD); it was prepared (24) and lentiviral particles were generated as described previously (25).

Lentiviral Infection of PTECs and Cellular Oxygen Consumption

The cellular bioenergetics profile of primary human PTECs was assessed using the Seahorse XF24 Flux Analyzer (Seahorse Bioscience, North Billerica, MA) (26). Human primary PTECs were seeded into 24-well XF24 cell culture microplates (Seahorse Bioscience) at 50,000 cells/well. Six hours later, cells were infected with lentivirus expressing AIF at a multiplicity of infection of 20 for 18 h with the addition of 5 μg/mL polybrene, and then were left to recover for 24 h in renal epithelial cell basal medium. Cells were washed and incubated at 37°C in DMEM containing either 5 mmol/L glucose, 1 mmol/L pyruvate, and 1 mmol/L glutamate or 25 mmol/L glucose, 1 mmol/L pyruvate, and 1 mmol/L glutamate, pH 7.4, for 2 h. Three basal OCR measurements were performed, and these were then repeated following sequential exposure to the ATP synthase inhibitor oligomycin (1 μmol/L), the proton ionophore FCCP (1 μmol/L), and the complex III inhibitor antimycin A (1 μmol/L). Calculations of the respiratory parameters of mitochondrial function were then completed (27). At the end of the assay, the number of cells was determined in each well using the CyQuant Cell Proliferation Assay kit (Molecular Probes) according to the instructions of the manufacturer.

AIF Immunohistochemistry of Human Renal Biopsy Material

The study was approved by the Human Research Ethics Committee at Austin Health and was conducted according to the principles of the Declaration of Helsinki. AIF immunohistochemistry was performed on clinically indicated renal biopsy samples collected from patients with DN (type 1 diabetes, $n = 2$, or type 2 diabetes, $n = 13$) and in age-matched (66 ± 7 vs. 68 ± 2 years, respectively) healthy kidney tissue sections obtained from nephrectomy for renal carcinoma or from donor kidneys ($n = 6$) before transplantation. The sections were incubated overnight in primary antibody (1:250; mouse anti-human AIF, catalog #sc-13116; Santa Cruz Biotechnology). The sections were then sequentially exposed to biotinylated horse anti-mouse IgG (Vector Laboratories, Burlingame, CA) followed by ABC Elite (Vector Laboratories), and then were visualized by 3,3-diaminobenzidine. Total cortical AIF was quantitated by computer-aided densitometry (Optimus 6.5; Media Cybernetics, Silver Springs, MD), as described previously (18). Fraction positivity for AIF in at least 40 randomly selected tubule cross sections per renal biopsy specimen was quantified using NIS-Elements imaging software (Nikon Instruments Inc.).

AIFM1 Gene Expression in Human Renal Biopsy Material

RNA was extracted from formalin-fixed, paraffin-embedded tissue specimens from 43 kidney biopsies performed in patients with diagnosed DN and from 16 kidneys from normal donors, and quantitative RT-PCR was performed as previously described (28) for *AIFM1* gene expression (Assay ID Hs.58.38539266; Integrated DNA Technologies, Coralville, IA). The primer and probe nucleotide sequences are shown in Supplementary Table 1. This assay detects all variants of *AIFM1*.

Statistics

All statistical computations were performed using Prism version 6.0 for Mac OSX (GraphPad Software, San Diego, CA). Values for experimental groups are given as the mean, with bars showing the SEM, unless otherwise stated. A Student *t* test was used to compare means between two groups. If data were nonparametric, a Mann-Whitney test was used. One-way ANOVA with Tukey post-test was used to determine statistical significance for three or more groups, where nonparametric data were logarithmically transformed before analysis. In some instances, two-way ANOVA with Bonferroni post hoc testing was used. Pearson coefficients were calculated for associations between variables. A P value of <0.05 was considered to be statistically significant.

RESULTS

AIF Is Expressed in Human Kidneys and Is Decreased in CKD

AIF was localized to renal cortical tubules both in kidneys from patients with CKD (DN) (Fig. 1*A*, arrows) (DN1–DN3) and in healthy kidney tissue sections (Fig. 1*A*) (ND1–ND3). The clinical characteristics of these individuals are shown in Supplementary Table 2. There was a fourfold decrease in renal cortical AIF protein content in renal biopsy samples from patients with CKD ($n = 15$ individuals with DN) when compared with samples from control subject kidneys ($n = 6$ individuals) (Fig. 1*B*) ($P < 0.001$). AIF protein content of the tubular compartment (per tubule cross section) was decreased by 50% (Fig. 1*C*) ($P < 0.002$), which was positively associated with declining eGFR (Fig. 1*D*).

To further confirm a decrease in AIF in the diabetic kidney, *AIFM1* mRNA expression was determined in a separate cohort of normal donor control kidneys ($n = 16$) and in renal biopsy samples from patients with DN ($n = 43$) by qPCR. Renal cortical expression of *AIFM1* was

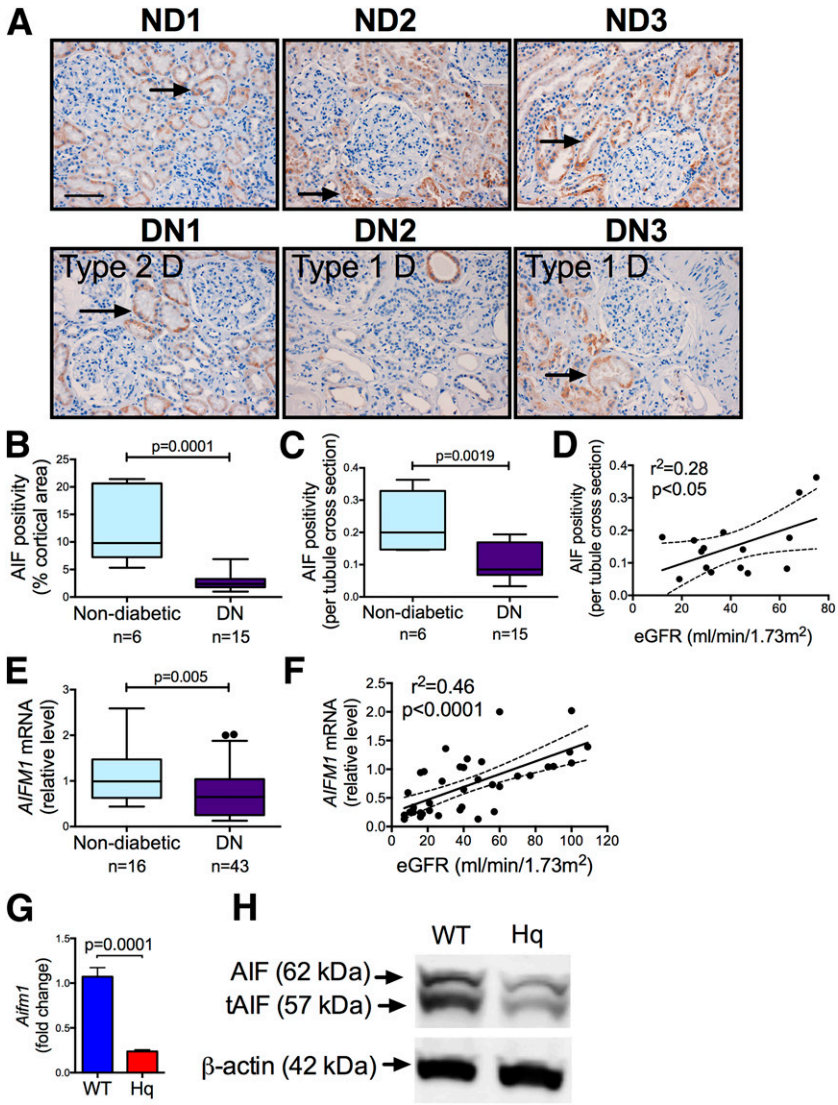

Figure 1—AIF is present in the human kidney and is decreased in patients with CKD. *A*: AIF was localized predominantly to the renal tubules in human renal biopsy samples obtained from individuals without diabetes (top panels, nondiabetic [ND1, ND2, ND3]) and from patients with diabetes and DN (DN1, DN2, DN3; bottom panels: left, type 2 diabetes; middle and right, type 1 diabetes). Original magnification ×200. Scale bar = 50 μm. Arrows indicate tubular AIF staining. *B*: Quantitation of AIF protein expression (percent cortical area) in patients with diabetes (n = 15) compared with individuals with normal glucose tolerance (n = 6), P = 0.0001. The box represents the interquartile range, whiskers represent range, and median is shown by the cross bar. *C*: Quantitation of AIF protein in renal tubules (per tubule cross section) in patients with diabetes (n = 15) compared with individuals with normal glucose tolerance (n = 6), P = 0.0019. *D*: Correlation between AIF (per tubule cross section) and eGFR, r^2 = 0.28, P = 0.042, n = 15 (data shown comprise n = 2 control subjects and n = 14 patients with diabetes). *E*: *AIFM1* mRNA expression by qPCR in renal cortex obtained from patients with DN (n = 43) and nondiabetic control subjects (n = 16), P = 0.005. *F*: Correlation between *AIFM1* gene expression and eGFR, r^2 = 0.46, P < 0.001, n = 38 (data comprise patients with DN only). *G*: *Aifm1* expression (encoding for AIF) in kidneys from Hq mice (n = 15) compared with WT control mice (n = 13). *H*: Representative immunoblots demonstrating mature (62 kDa) and truncated AIF (tAIF; 57 kDa) protein with β-actin loading control in kidney cortical homogenates from WT and *Aifm1*$^{Hq/Y}$ (Hq) mice.

decreased in individuals with DN, compared with healthy donors (Fig. 1*E*) ($P < 0.01$), and also positively correlated with eGFR (Fig. 1*F*).

Knockdown of AIF Phenocopies CKD

To determine whether decreases in AIF could be a primary cause of CKD, we studied the *Aifm1*$^{Hq/Y}$ mouse, which harbors a retroviral insertion in the *Aifm1* gene encoding AIF, resulting in partial knockdown of AIF (13). At week 18 of life, both *Aifm1* gene expression (Fig. 1*G*) and mature and truncated forms of the AIF protein (Fig. 1*H*) were significantly decreased in the kidney cortices of *Aifm1*$^{Hq/Y}$ mice when compared with those of control mice. Partial knockdown of AIF in *Aifm1*$^{Hq/Y}$ mice led to a decrease in body weight and renal hypertrophy, but did not change fasting blood glucose or GHb concentrations

(Table 1). *Aifm1*$^{Hq/Y}$ mice had increased urinary albumin excretion rates (AERs) (Fig. 2*A*) as well as renal structural damage, including glomerulosclerosis (Fig. 2*B* and *C*) and collagen IV deposition (Fig. 2*D* and *F*). In concert with glomerular lesions, there was expansion of the tubulointerstitial compartment, including collagen IV deposition (Fig. 2*E* and *F*), increased tubulointerstitial area (Fig. 2*G*), and shedding of the ectodomain of the epithelial cell adhesion molecule KIM-1 into the urine (Fig. 2*H*), which is consistent with proximal tubular injury (29,30). Knockdown of AIF in the absence of diabetes also resulted in hyperfiltration, as indicated by an increase in creatinine clearance (Fig. 2*I*), and a decrease in plasma cystatin C (Fig. 2*J*) (31). Finally, urinary excretion of NGAL (32), which is indicative of tubular damage, was increased with AIF knockdown (Fig. 2*K*).

Mitochondrial Bioenergetics Are Altered With AIF Knockdown, Independent of Changes in Complex I Activity or Assembly

In *Aifm1*$^{Hq/Y}$ mice, a disturbance in bioenergetics was evident, including a marked increase in mitochondrial ATP content (Supplementary Fig. 1*A*). In parallel experiments, renal mitochondrial respiration was determined using OCR in the presence of the complex I substrates glutamate and malate (Supplementary Fig. 1*B*). Complex I–driven basal and ADP-stimulated (state III) OCR were not different between control and *Aifm1*$^{Hq/Y}$ mice. However, state IV and uncoupled dinitrophenol complex I–driven OCR were increased in renal mitochondria from *Aifm1*$^{Hq/Y}$ mice (Supplementary Fig. 1*B*). Mitochondrial respiration in the presence of the complex II substrate succinate and rotenone (to inhibit complex I and thus reverse electron transport) was not different between control and *Aifm1*$^{Hq/Y}$ mice (Supplementary Fig. 1*C*).

Complex I–driven mitochondrial superoxide production (Supplementary Fig. 1*D*) was increased in the face of compensatory increases in the activity of manganese superoxide dismutase (Supplementary Fig. 1*E*) in mitochondria from *Aifm1*$^{Hq/Y}$ mouse kidneys. The expression of NADPH oxidase isoform-4 (*Nox4*), a key source of kidney reactive oxygen species, including from mitochondria (33), was also elevated in the renal cortex (Supplementary Fig. 1*F*). Despite a 50% lower AIF protein content in the kidney, renal mitochondrial complex I activity was not different in *Aifm1*$^{Hq/Y}$ mice at week 10 (Supplementary Fig. 1*G*). Blue native PAGE on renal mitochondrial extracts, using 1% digitonin solubilization to examine respiratory chain supercomplexes, revealed no differences in complex I supercomplex assembly among groups (Supplementary Fig. 1*H*). Further, 1% Triton X-100 dissociation of supercomplexes into smaller complexes and holo-complexes (34) also showed no differences among groups (Supplementary Fig. 1*I*). There were also no changes in supercomplex assembly of complexes III, IV, or V (data not shown).

AIF Knockdown Induces Mitochondrial Fusion Events

Transmission electron microscopy showed mitochondria of a mixed population in PTECs (Fig. 3*A*, left), that is, fragmented, intermediate, and elongated. However, mitochondria in PTECs of *Aifm1*$^{Hq/Y}$ mice appeared more elongated (Fig. 3*A*, right). This elongation was confirmed by the assessment of mitochondrial length, which was significantly increased in *Aifm1*$^{Hq/Y}$ compared with WT mice (Fig. 3*B*). The aspect ratio of mitochondria, which takes into account both length and width, was also increased in *Aifm1*$^{Hq/Y}$ mice (Fig. 3*C*). PTECs of *Aifm1*$^{Hq/Y}$ mice also had fewer mitochondria per field than WT mice (Fig. 3*D*).

Western immunoblotting of the protein guanosine triphosphatase OPA1 demonstrated that long isoforms 1 and 2 (L1 and L2) and three short isoforms (S1, S2, and S3) (35) were detected in kidneys of WT and *Aifm1*$^{Hq/Y}$ mice (Fig. 3*E*). While there was no change in the abundance of fusion-associated L1 and L2, all three short isoforms of OPA1, which relate to fission events, were decreased in the renal cortices of nondiabetic *Aifm1*$^{Hq/Y}$ mice compared with WT mice (Fig. 3*E*, right). MFN1 and MFN2, which regulate outer mitochondrial membrane fusion (36), were increased in the renal cortex of *Aifm1*$^{Hq/Y}$ mice (Fig. 3*F*). When taken together, these changes show a shift toward mitochondrial fusion in renal mitochondria with AIF deficiency. Gene expression of *Ppargc1α* (Fig. 3*G*) and *Tfam* (Fig. 3*H*) was not changed, suggesting that mitochondrial biogenesis is not altered by AIF knockdown.

Superimposition of Diabetes on *Aifm1* Knockdown Worsens Kidney Damage by Extensive Changes in Mitochondrial Networking

DN is a leading cause of end-stage renal disease, and alterations in mitochondrial bioenergetics and dynamics

Table 1—Phenotypic and biochemical characteristics of mice

	WT	Hq	WT diabetic	Hq diabetic
BW (g)	35 ± 4	23 ± 3*	25 ± 2*	22 ± 2*
Kidney weight/BW ($\times 10^{-2}$)	1.1 ± 0.1	1.7 ± 0.6*	1.9 ± 0.3*	1.7 ± 0*†
FBG (mmol/L)	10.4 ± 3.1	11.2 ± 5.2	28.5 ± 8.2*	24.2 ± 7.2*†
GHb (%)	3.9 ± 0.1	3.8 ± 0.1	7.9 ± 1.0	8.0 ± 0.5

Data are reported as the mean ± SEM. Male mice (n = 20/group) were studied from week 8 to week 18 of life. *$P < 0.05$ vs. WT mice. †$P < 0.05$ vs. WT diabetic mice. BW, body weight; FBG, fasting blood glucose; Hq, *Aifm1*$^{Hq/y}$.

in the kidney in experimental diabetes have been documented (4,37,38). Hence, we superimposed diabetes onto AIF knockdown in mice to determine whether the renal phenotype could be worsened. In kidneys from diabetic WT mice, the truncated isoform of AIF was decreased compared with kidneys from WT mice (Supplementary Fig. 2*B* and *C*), whereas both the mature and truncated isoforms were decreased in *Aifm1*$^{Hq/Y}$ diabetic mice (Supplementary Fig. 2*A*–*C*). As expected, diabetic WT mice developed renal injury, and this was similar to that seen in the nondiabetic *Aifm1*$^{Hq/Y}$ mice. With diabetes, urinary AERs were increased, and this was exacerbated in diabetic *Aifm1*$^{Hq/Y}$ mice (Fig. 4*A*). In the kidney, there was glomerulosclerosis (Fig. 4*B*), deposition of glomerular (Fig. 4*C*) and tubular collagen IV (Fig. 4*D*), and urinary excretion of KIM-1 (Fig. 4*E*), which were further increased in diabetic *Aifm1*$^{Hq/Y}$ mice. By contrast, expression of the extracellular matrix protein fibronectin (*Fn1*) was elevated by both *AIF* deficiency and diabetes, and this was not augmented in diabetic *Aifm1*$^{Hq/Y}$ mice (Fig. 4*F*). Diabetic *Aifm1*$^{Hq/Y}$ mice had a further decrease in plasma cystatin C when compared with both WT diabetic and nondiabetic *Aifm1*$^{Hq/Y}$ mice (Fig. 4*G*), indicating renal hyperfiltration. Creatinine clearance was increased by the same degree in all groups when compared with WT mice (Fig. 4*H*).

Diabetic mice had decreased mitochondrial ATP content in the kidney cortex, which was further exacerbated by AIF knockdown (Fig. 4*I*). Mitochondrial superoxide production (Fig. 4*J*) was not changed by diabetes in WT or *Aifm1*$^{Hq/Y}$ mice. However, there was evidence of electron flux to peroxynitrite in the diabetic setting, demonstrated by increased mitochondrial 3-NT content, which was further increased in diabetic *Aifm1*$^{Hq/Y}$ mice (Fig. 4*K*). Renal cortical *Nox4* expression was also elevated in diabetic *Aifm1*$^{Hq/Y}$ mice compared with other groups (Fig. 4*L*).

By imaging with an electron microscope, it was seen that mice with diabetes had an increase in mitochondrial fragmentation within PTECs compared with WT control mice (Fig. 5*A*). This change was verified by a decrease in the aspect ratio (length/width) of mitochondria (Fig. 5*B*). Diabetic *Aifm1*$^{Hq/Y}$ mice showed a greater number of fragmented mitochondria in their renal cortices, as supported by a decrease in the aspect ratio (Fig. 5*A* and *B*). This was accompanied by an increase in recruitment of the guanosine triphosphatase Drp-1 to mitochondria (Fig. 5*C* and

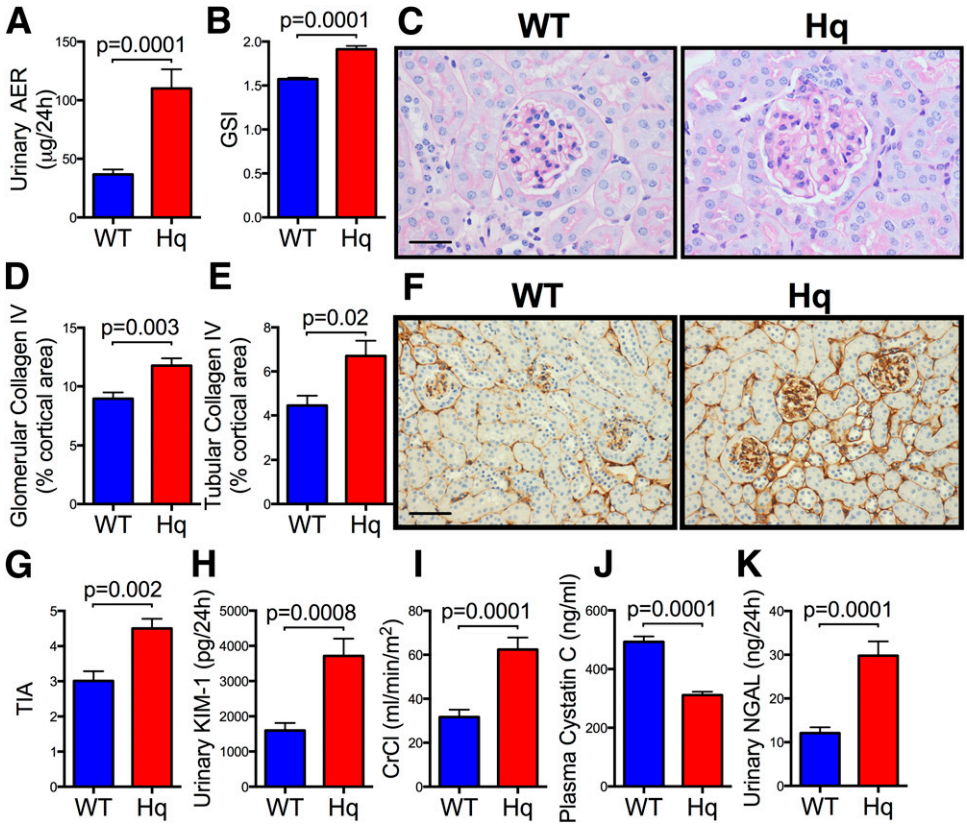

Figure 2—Knockdown of AIF recapitulates nephropathy. Urinary AER (*A*), GSI (*B*), photomicrographs of PAS-stained renal cortex (original magnification ×400, scale bar = 25 μm) (*C*), quantitation of collagen IV deposition within glomeruli (*D*), quantitation of collagen IV deposition within the tubulointerstitial compartment (*E*), photomicrographs of collagen IV deposition by immunohistochemistry (original magnification ×200, scale bar = 50 μm) (*F*), tubulointerstitial area (TIA) (*G*), urinary excretion of KIM-1 (*H*), creatinine clearance (CrCl) (*I*), and plasma cystatin C level (*J*). *K*: Urinary excretion of NGAL. Data are reported as the mean ± SEM, *n* = 5–15 mice/group. *Aifm1*$^{Hq/Y}$, Hq.

D), suggesting increased mitochondrial fission in kidneys taken from the diabetic *Aifm1*$^{Hq/Y}$ group. While the level of mitochondrial fusion protein MFN1 was not changed in diabetic kidneys (Fig. 5*E* and *F*), that of MFN2 was increased (Fig. 5*E* and *G*) and OPA1 expression was unchanged (Fig. 5*H*).

Supporting an increase in fission, diabetes increased the expression of renal mitochondrial fission factor (Fig. 5*I*), which facilitates the recruitment of Drp-1 to the mitochondrial surface (39), in *Aifm1*$^{Hq/Y}$ mice. *Ppargc1α* expression was also elevated by diabetes (Fig. 5*J*), but there was a corresponding decrease in *Tfam* expression (Fig. 5*K*).

Gain of Function in AIF Restores OXPHOS in Human Primary PTECs After Exposure to High Glucose

High-glucose treatment in PTECs decreased AIF gene expression, which was not seen with the osmotic control (5 mmol/L D-glucose and 20 mmol/L mannitol) (Fig. 6*A*). Next, we performed lentiviral overexpression of AIF in primary PTECs using the delivery vector cFugw-AIF (Fig.

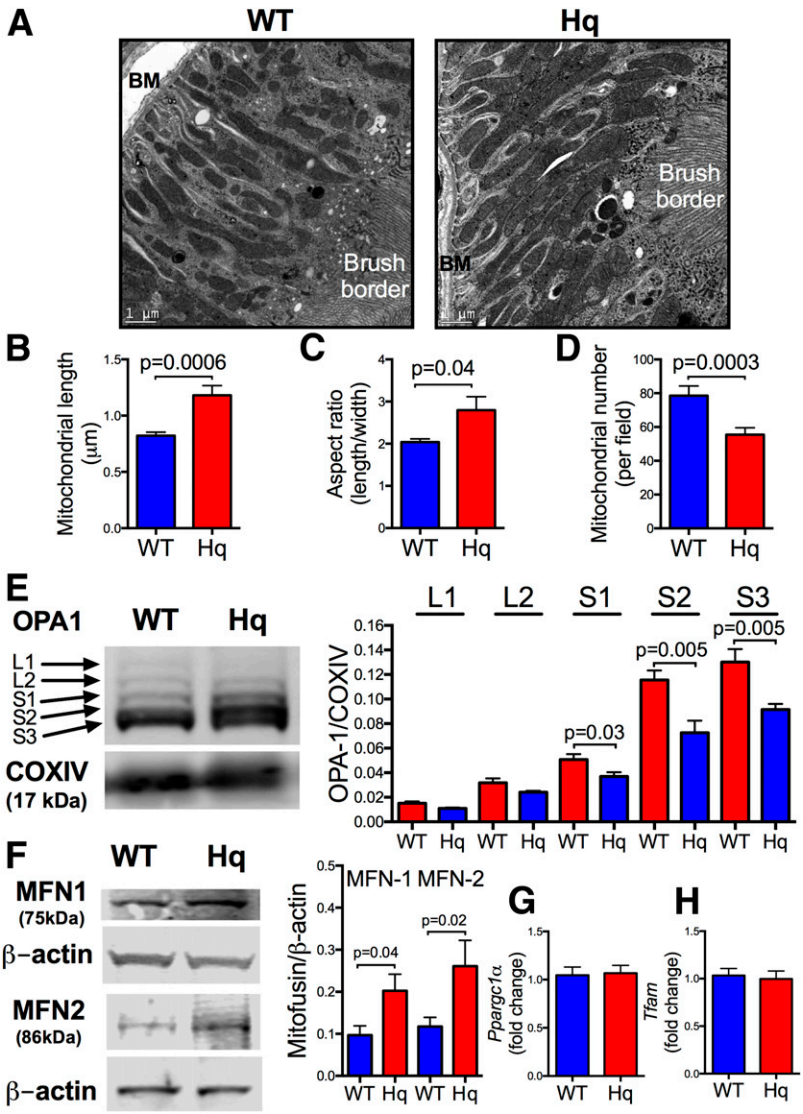

Figure 3—AIF knockdown mediates mitochondrial fusion events. *A*: Electron micrographs of renal PTECs showing mitochondrial morphology in WT (left) and Hq (right) mice. BM, basement membrane. Original magnification ×15,000. Scale bar = 1 μm. *B*: Mitochondrial length measured using ImageJ. Data are reported as the mean ± SEM, *n* = 5–6 images/mouse (with up to 115 mitochondria scored in each image), *n* = 3 mice/group. *C*: Mitochondrial aspect ratio (length/width). Data are mean ± SEM, *n* = 5–6 images/mouse (with up to 115 mitochondria scored in each image), *n* = 3 mice/group. *D*: Mitochondrial number per field. Data are the mean ± SEM, *n* = 5–6 images/mouse, *n* = 3 mice/group. *E*, Left: Representative Western blot (gradient gel) of OPA1 in showing the five isoforms: long isoforms 1 and 2 (L1 and L2) and short isoforms 1–3 (S1, S2, and S3) (spanning 80–100 kDa). COX IV loading control (bottom). Right: Quantitation of OPA1 Western blot, *n* = 8 mice/group. *F*, Left: Representative Western blot of MFN1 and MFN with β-actin loading controls beneath. Right: Quantitation of MFN1 and MFN2 Western blots relative to β-actin, *n* = 6–8 mice/group. qPCR analysis of genes involved in mitochondrial biogenesis: *Ppargc1α* (*G*) and *Tfam* (*H*) in renal cortex of WT mice and *Aifm1*$^{Hq/Y}$ (Hq) mice. *n* = 14 mice/group.

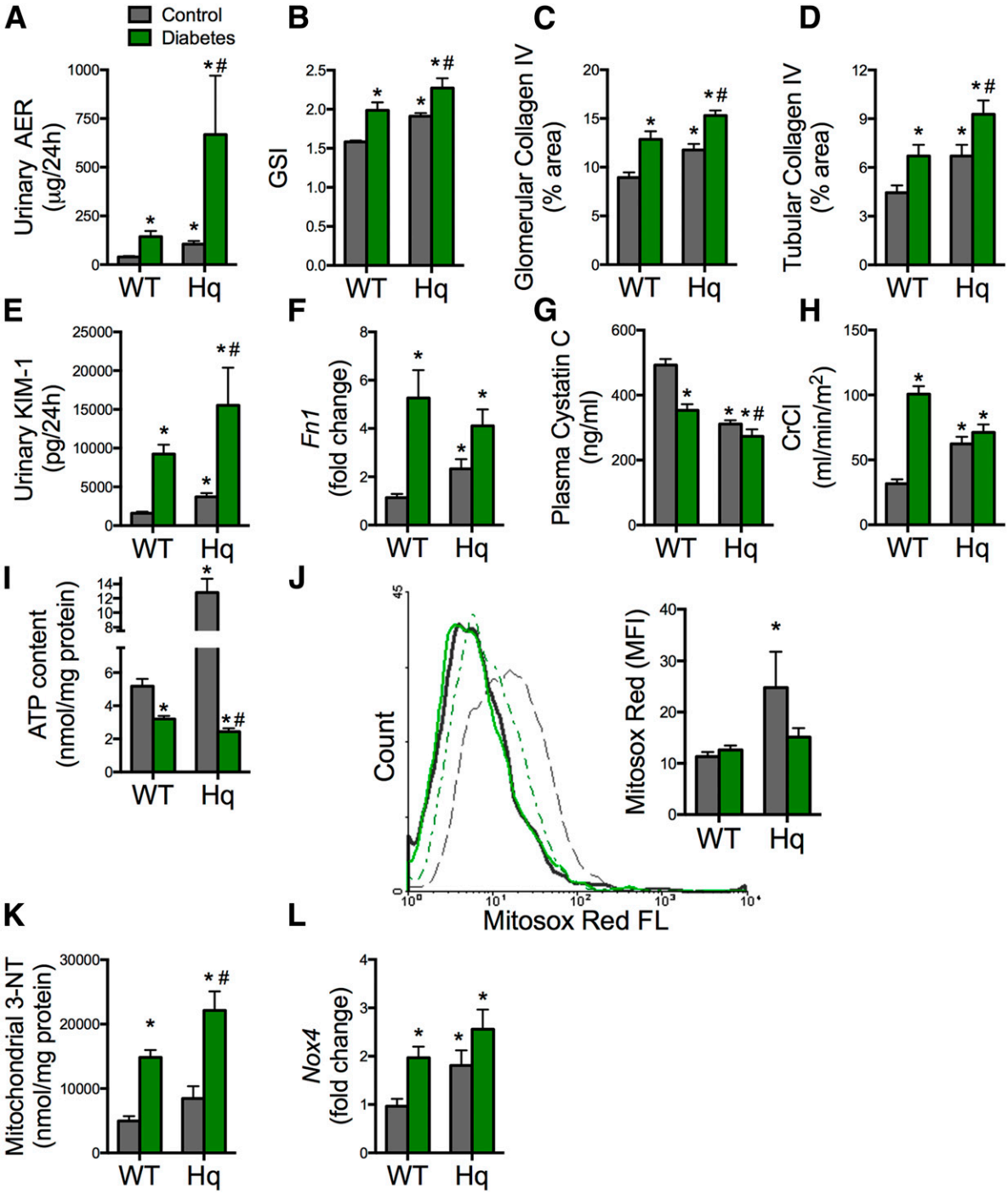

Figure 4—Diabetes superimposition on *Aifm1* knockdown worsens renal pathology. Diabetes was induced in WT and *Aifm1*$^{Hq/Y}$ (Hq) mice by streptozotocin. Urinary AER (*A*), GSI (*B*), quantitation of glomerular collagen IV (*C*), quantitation of tubulointerstitial collagen IV (*D*), urinary excretion of KIM-1 (*E*), *Fn1* mRNA expression (*F*), plasma cystatin C (*G*), creatinine clearance (CrCl) (*H*), and renal mitochondrial ATP content (*I*). *J*: Representative histogram of mitochondrial superoxide production using the Mitosox Red probe (5 μmol/L) with detection by flow cytometry: WT control mice (gray solid line), *Aifm1*$^{Hq/Y}$ (Hq) control mice (gray dotted line), WT diabetic mice (green solid line), and *Aifm1*$^{Hq/Y}$ (Hq) diabetic mice (green dotted line). Inset: Quantification of the flow cytometry data (n = 5 mice/group). FL, fluorescence; MFI, mean fluorescence intensity. *K*: Mitochondrial 3-NT. *L*: *Nox4* mRNA expression in renal cortex. *P < 0.05 compared with WT control, #P < 0.05 compared with Hq control. Data are reported as the mean ± SEM, n = 5–15 mice/group.

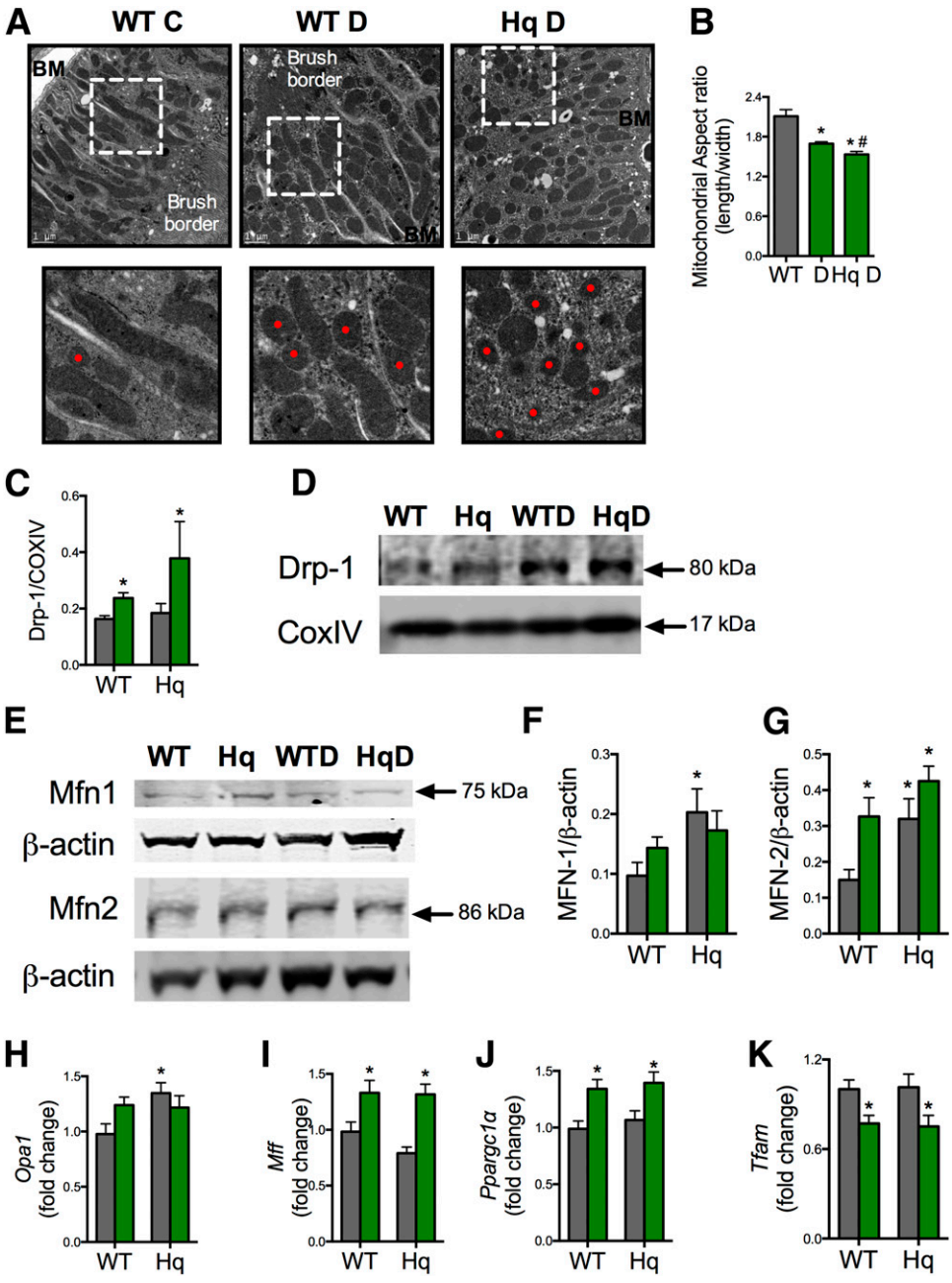

Figure 5—Diabetes superimposition on *Aifm1* knockdown remodels the mitochondrial network. *A*: Electron micrographs of renal PTECs showing mitochondrial morphology in WT control (left), WT diabetic (middle), and *Aifm1*$^{Hq/Y}$ (Hq) diabetic (right) mice. Red dots indicate fragmented mitochondria. BM, basement membrane. Top row: Original magnification ×15,000; scale bar = 1 μm. Bottom row is the area bounded by the white boxes in the top row enlarged. *B*: Mitochondrial aspect ratio (length/width). The gray bar represents control mice, and the green bars represent mice with diabetes (D). Data are reported as the mean ± SEM, *n* = 5–6 images/mouse (with up to 143 mitochondria scored in each image), *n* = 3 mice/group. *C*: Quantitation of Western blot of Drp-1 in mitochondrial isolates, *n* = 4 mice/group. COX IV was used as a loading control. *D*: Representative Western blot of Drp-1 (80 kDa) in mitochondria with COX IV loading control, *n* = 4 mice/group. *E*: Representative Western blots of MFN1 and MFN2 with corresponding β-actin loading controls beneath. *F*: Quantitation of MFN1 Western blot relative to β-actin, *n* = 6–8 mice/group. *G*: Quantitation of MFN2 Western blots relative to β-actin, *n* = 6–8 mice/group. qPCR analysis of genes involved in mitochondrial fusion, fission, and biogenesis *Opa1* (*H*); mitochondrial fission factor (*Mff*) (*I*); *Ppargc1α* (*J*); and *Tfam* renal cortex (*K*). *n* = 9–15 mice/group. *$P < 0.05$ compared with WT control mice, #$P < 0.01$ compared with diabetic mice.

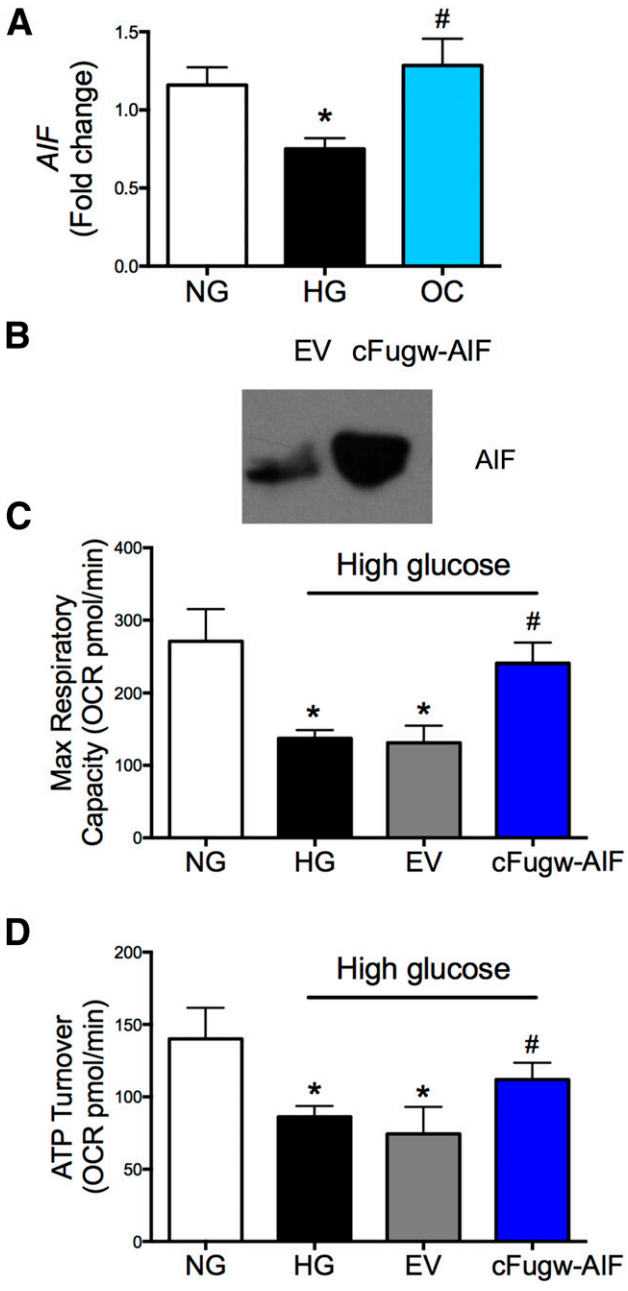

Figure 6—AIF overexpression restores OXPHOS in human primary PTECs. *A*: Primary human PTECs were exposed to 5 mmol/L D-glucose (normal glucose [NG]), 25 mmol/L D-glucose (high glucose [HG]), or 5 mmol/L D-glucose plus 20 mmol/L mannitol (osmotic control [OC]) for 48 h, and AIF mRNA expression was measured by qPCR; n = 3 replicates/group and two independent cell culture experiments. *P < 0.05 compared with NG-treated cells. #P < 0.05 compared with HG-treated cells. *B*: Western blot showing efficiency of lentiviral overexpression of AIF. EV, empty vector. cFugw-AIF, AIF lentivirus. *C* and *D*: Human primary PTECs were exposed to NG or HG with or without overexpression of AIF by lentiviral infection. Cellular respiration (OCR) was measured using a Seahorse XF24 Bioanalyzer to determine maximal respiratory capacity (*C*) and ATP turnover/20,000 cells (*D*). n = 6 replicates/group with two independent cell culture experiments. Max, maximum. *P < 0.05 compared with NG-treated cells. #P < 0.05 compared with HG-treated cells.

6*B*). Metabolic profiling using a Seahorse XF24 Bioanalyzer showed that high glucose induced a decrease in OCR maximal respiratory capacity (Fig. 6*C*) and ATP turnover (Fig. 6*D*), which was rescued by the overexpression of AIF.

DISCUSSION

The current studies have demonstrated that partial knockdown of AIF leads to renal injury, including glomerular and tubulointerstitial damage and hyperfiltration. This phenotype was associated with changes in mitochondrial dynamics and bioenergetics, including excess mitochondrial superoxide production, a markedly increased ATP pool, and an increase in mitochondrial fusion. There was, however, no loss of complex I activity or assembly despite a 50% lower AIF protein expression in the kidney. When diabetes was superimposed on AIF deficiency, the changes in mitochondrial networking were more extensive, with mitochondrial fragmentation and depletion of the renal ATP pool, which augmented both the structural and functional abnormalities seen in the kidney. Furthermore, significant depletion of AIF protein within tubules and a decrease in *AIFM1* gene expression were evident in renal biopsy samples taken from patients with DN compared with healthy control subjects. Finally, lentiviral overexpression of AIF rescued glucose-induced disruption of cellular respiration in human primary proximal tubule cells. Taken together, these studies suggest that AIF deficiency leading to mitochondrial dysfunction is a risk factor for DN.

In these studies, AIF deficiency in the absence of diabetes led to kidney injury, which resembled early DN, including aberrant mitochondrial bioenergetics and dynamics in the kidney. Within the renal cortices from $Aifm1^{Hq/Y}$ mice, with AIF deficiency, ATP content was increased, indicating that a partial loss of AIF may drive a compensatory change in mitochondrial dynamics, with an increase in fusion. This is consistent with previous studies showing that fusion events increase ATP generation (40,41). A physical interaction between OPA1 and AIF has also been described, although it is unclear whether this occurs to facilitate mitochondrial fusion events (42). Our data show that AIF knockdown decreased the specific isoforms of OPA1, which is responsible for mitochondrial fission (35), but increased other mitochondrial fusion proteins, MFN1 and MFN2 (36), in kidneys from nondiabetic $Aifm1^{Hq/Y}$ mice. Given the increase in mitochondrial length, aspect ratio, and a decrease in mitochondrial number, there was an increase in mitochondrial fusion within the renal tubules of nondiabetic $Aifm1^{Hq/Y}$ mice, which was associated with an increase in ATP content. We would therefore suggest that this compensatory increase in ATP as a result of fusion events is present early in renal injury but that, as disease progresses, ATP concentrations cannot be sustained at sufficient levels, leading to further renal injury and cell death. Intriguingly, however, mitochondrial fusion,

leading to increased renal ATP content at week 16, did not prevent the early renal functional and structural injury observed in the nondiabetic *Aifm1*$^{Hq/Y}$ mice. This suggests that rather than being compensatory, the early increase in ATP may represent a defect in ATP use at this time, setting the stage for further renal injury. This concept should be investigated in future studies.

There is evidence to indicate that AIF is important in the maintenance of mitochondrial structure (43). Cheung et al. (43) found that neurons with severely depleted AIF have reduced viability, abnormally dilated mitochondrial cristae, and mitochondrial fragmentation. In the current study, a worsening of renal injury with diabetes was seen in mice with AIF deficiency, in association with fragmentation of mitochondria within the tubular compartment. This was also supported by increased recruitment of the fission protein Drp-1 to renal mitochondria taken from *Aifm1*$^{Hq/Y}$ mice with diabetes. Previous studies have demonstrated that fragmentation of mitochondria within the kidney is linked to both acute (44) and chronic (37,45,46) renal injury and that it is likely that this is the reason for the inability of the diabetic *Aifm1*$^{Hq/Y}$ mice to maintain an adequate renal ATP pool. In agreement with this, we showed that interruption of OXPHOS in human PTECs by high glucose levels was prevented by the restoration of AIF protein, which also rescued ATP turnover.

There have been several previous reports (15) suggesting that AIF plays a role in the assembly of complex I of the mitochondrial electron transport chain. However, the effects may be tissue specific, since previous studies have observed a variable impact of AIF mutations on complex I activity (15,47), including the finding that decreasing AIF did not change complex I assembly, supercomplex formation, or activity. However, recently, a study (48) of two related patients with loss-of-function mutations in *AIFM1*, which affected both redox and DNA-binding properties of the AIF protein, showed no evidence of complex I deficiency in mitochondria taken from their skin fibroblasts or skeletal muscle biopsy samples.

AIF is encoded as a 67-kDa protein that contains a mitochondrial localization signal. Upon import into the mitochondria, the mitochondrial localization signal is removed, generating the mature 62-kDa protein, which is N-terminally anchored to the inner mitochondrial membrane (49). The mature form comprises a flavin adenine dinucleotide–binding domain and an NADH-binding domain, which are thought to confer electron transfer activity (12), as well as a COOH-terminal domain (50). A truncated isoform of the protein (57 kDa) is also generated in the intermembrane space after proteolytic processing, which is thought to be mediated by μ-calpain, a cysteine protease (50). This isoform also contains the flavin adenine dinucleotide–binding domain, NADH-binding domain, and a COOH-terminal domain and, as such, likely retains oxidoreductase activity. *Aifm1*$^{Hq/Y}$ mice also had concomitant decreases in mature AIF and the gene expression of *Aifm1*, and had worse kidney disease than their WT littermates. In our human samples, obtained from individuals with diabetes who had advanced DN, we also showed that both total AIF protein and expression of the *AIF* gene were decreased in kidney cortices. Hence, we have postulated that decreased gene expression leading to a decrease in both isoforms of AIF results in more advanced kidney disease. However, it is also evident that a decline in truncated AIF alone, as seen in the WT diabetic mice, can also impair kidney function and cause structural damage to the kidney. This warrants further investigation in future studies.

Taken together, these studies demonstrate that a deficiency in AIF results in changes in mitochondrial function, networking, and reactive oxygen species production, which could precipitate renal disease. In the presence of diabetes, a switch from mitochondrial fusion to fission, impaired OXPHOS, and a depleted mitochondrial ATP pool lead to more advanced renal injury. These studies support a novel role for the AIF protein in the maintenance of kidney function via the control of mitochondrial homeostasis and ATP generation. Future studies should focus on upstream regulators leading to AIF depletion in the kidney during diabetes, which could ultimately lead to new therapeutic targets relevant to DN.

Acknowledgments. The authors thank Amy Morley, Felicia Yap, Anna Gasser, Edward Grixti, and Maryann Arnstein (Baker IDI Heart and Diabetes Institute) for their technical expertise. The authors also thank Drs. Valina and Ted Dawson (The Johns Hopkins University School of Medicine) for the AIF plasmid. In addition, the authors thank Joan Clarke (Monash University) for assistance with electron microscopy and Dr. Lydia Wong and Michele Milne (The University of Melbourne) for data retrieval and collation.

Funding. This work was completed with support from the National Health and Medical Research Council of Australia (NHMRC) (grant APP1023664) and the Victorian Government's Operational Infrastructure Support Program. M.T.C. has been supported by the Australian Diabetes Society Skip Martin Early Career Fellowship and the Australian and New Zealand Society of Nephrology Career Development Fellowship. G.C.H. is supported by a postdoctoral fellowship from JDRF. D.C.H. and L.A.G. have been supported by postdoctoral fellowships from the NHMRC/National Heart Foundation of Australia. S.L.M. is supported by an NHMRC Career Development Fellowship. M.T.R., M.E.C., D.R.T., and J.M.F. are NHMRC Research Fellows.

Duality of Interest. No potential conflicts of interest relevant to this article were reported.

Author Contributions. M.T.C. conceived and designed the study, performed data analysis and interpretation, provided financial support, and wrote the article. G.C.H. performed experiments and data analysis and interpretation. T.-V.N., S.A.P., V.T.-B., S.M.T., G.R., N.J.V.B., D.C.H., K.C.S., B.E.H., I.A.T., P.M.R., A.L., S.L.M., A.J.G., K.W., B.G.D., P.G., H.Q., M.C.T., X.W.W., L.A.G., and M.H.-E. performed experiments and data analysis. G.J., R.J.M., A.S., D.A.P., and E.I.E. provided human renal biopsy material and associated data. M.T.R. and D.R.T. conceived and designed the study and performed data interpretation. M.E.C. provided financial support and performed data interpretation. J.M.F. performed conception and design, provided financial support, performed data analysis and interpretation, and wrote and provided final approval of the article. M.T.C. is the guarantor of this work and, as such, had full access to all the data in the study and takes responsibility for the integrity of the data and the accuracy of the data analysis.

Prior Presentation. Parts of this study were presented in abstract form at the 75th Scientific Sessions of the American Diabetes Association, Boston, MA, 5–9 June 2015.

References

1. Soltoff SP. ATP and the regulation of renal cell function. Annu Rev Physiol 1986;48:9–31
2. Forbes JM, Ke BX, Nguyen TV, et al. Deficiency in mitochondrial complex I activity due to Ndufs6 gene trap insertion induces renal disease. Antioxid Redox Signal 2013;19:331–343
3. Kang HM, Ahn SH, Choi P, et al. Defective fatty acid oxidation in renal tubular epithelial cells has a key role in kidney fibrosis development. Nat Med 2015;21:37–46
4. Coughlan MT, Thorburn DR, Penfold SA, et al. RAGE-induced cytosolic ROS promote mitochondrial superoxide generation in diabetes. J Am Soc Nephrol 2009;20:742–752
5. Forbes JM, Coughlan MT, Cooper ME. Oxidative stress as a major culprit in kidney disease in diabetes. Diabetes 2008;57:1446–1454
6. Sharma K, Karl B, Mathew AV, et al. Metabolomics reveals signature of mitochondrial dysfunction in diabetic kidney disease. J Am Soc Nephrol 2013;24:1901–1912
7. Sivitz WI, Yorek MA. Mitochondrial dysfunction in diabetes: from molecular mechanisms to functional significance and therapeutic opportunities. Antioxid Redox Signal 2010;12:537–577
8. Daehn I, Casalena G, Zhang T, et al. Endothelial mitochondrial oxidative stress determines podocyte depletion in segmental glomerulosclerosis. J Clin Invest 2014;124:1608–1621
9. Che R, Yuan Y, Huang S, Zhang A. Mitochondrial dysfunction in the pathophysiology of renal diseases. Am J Physiol Renal Physiol 2014;306:F367–F378
10. Hall AM, Unwin RJ. The not so "mighty chondrion": emergence of renal diseases due to mitochondrial dysfunction. Nephron Physiol 2007;105:1–10
11. Susin SA, Lorenzo HK, Zamzami N, et al. Molecular characterization of mitochondrial apoptosis-inducing factor. Nature 1999;397:441–446
12. Miramar MD, Costantini P, Ravagnan L, et al. NADH oxidase activity of mitochondrial apoptosis-inducing factor. J Biol Chem 2001;276:16391–16398
13. Klein JA, Longo-Guess CM, Rossmann MP, et al. The harlequin mouse mutation downregulates apoptosis-inducing factor. Nature 2002;419:367–374
14. Bénit P, Goncalves S, Dassa EP, Brière JJ, Rustin P. The variability of the harlequin mouse phenotype resembles that of human mitochondrial-complex I-deficiency syndromes. PLoS One 2008;3:e3208
15. Vahsen N, Candé C, Brière JJ, et al. AIF deficiency compromises oxidative phosphorylation. EMBO J 2004;23:4679–4689
16. Tan AL, Sourris KC, Harcourt BE, et al. Disparate effects on renal and oxidative parameters following RAGE deletion, AGE accumulation inhibition, or dietary AGE control in experimental diabetic nephropathy. Am J Physiol Renal Physiol 2010;298:F763–F770
17. Saito T, Sumithran E, Glasgow EF, Atkins RC. The enhancement of aminonucleoside nephrosis by the co-administration of protamine. Kidney Int 1987;32:691–699
18. Thallas-Bonke V, Thorpe SR, Coughlan MT, et al. Inhibition of NADPH oxidase prevents advanced glycation end product-mediated damage in diabetic nephropathy through a protein kinase C-alpha-dependent pathway. Diabetes 2008;57:460–469
19. Coughlan MT, Yap FY, Tong DC, et al. Advanced glycation end products are direct modulators of β-cell function. Diabetes 2011;60:2523–2532
20. Drew B, Leeuwenburgh C. Method for measuring ATP production in isolated mitochondria: ATP production in brain and liver mitochondria of Fischer-344 rats with age and caloric restriction. Am J Physiol Regul Integr Comp Physiol 2003;285:R1259–R1267
21. Henstridge DC, Bruce CR, Drew BG, et al. Activating HSP72 in rodent skeletal muscle increases mitochondrial number and oxidative capacity and decreases insulin resistance. Diabetes 2014;63:1881–1894
22. Lee S, Sheck L, Crowston JG, et al. Impaired complex-I-linked respiration and ATP synthesis in primary open-angle glaucoma patient lymphoblasts. Invest Ophthalmol Vis Sci 2012;53:2431–2437
23. McKenzie M, Lazarou M, Thorburn DR, Ryan MT. Analysis of mitochondrial subunit assembly into respiratory chain complexes using Blue Native polyacrylamide gel electrophoresis. Anal Biochem 2007;364:128–137
24. Wang Y, Kim NS, Haince JF, et al. Poly(ADP-ribose) (PAR) binding to apoptosis-inducing factor is critical for PAR polymerase-1-dependent cell death (parthanatos). Sci Signal 2011;4:ra20
25. Nicholls PK, Stanton PG, Rainczuk KE, Qian H, Gregorevic P, Harrison CA. Lentiviral transduction of rat Sertoli cells as a means to modify gene expression. Spermatogenesis 2012;2:279–284
26. Martin SD, Morrison S, Konstantopoulos N, McGee SL. Mitochondrial dysfunction has divergent, cell type-dependent effects on insulin action. Mol Metab 2014;3:408–418
27. McGee SL, Sadli N, Morrison S, Swinton C, Suphioglu C. DHA protects against zinc mediated alterations in neuronal cellular bioenergetics. Cell Physiol Biochem 2011;28:157–162
28. Herman-Edelstein M, Scherzer P, Tobar A, Levi M, Gafter U. Altered renal lipid metabolism and renal lipid accumulation in human diabetic nephropathy. J Lipid Res 2014;55:561–572
29. Han WK, Bailly V, Abichandani R, Thadhani R, Bonventre JV. Kidney injury molecule-1 (KIM-1): a novel biomarker for human renal proximal tubule injury. Kidney Int 2002;62:237–244
30. Zhang Z, Humphreys BD, Bonventre JV. Shedding of the urinary biomarker kidney injury molecule-1 (KIM-1) is regulated by MAP kinases and juxtamembrane region. J Am Soc Nephrol 2007;18:2704–2714
31. Song S, Meyer M, Türk TR, et al. Serum cystatin C in mouse models: a reliable and precise marker for renal function and superior to serum creatinine. Nephrol Dial Transplant 2009;24:1157–1161
32. Viau A, El Karoui K, Laouari D, et al. Lipocalin 2 is essential for chronic kidney disease progression in mice and humans. J Clin Invest 2010;120:4065–4076
33. Jha JC, Gray SP, Barit D, et al. Genetic targeting or pharmacologic inhibition of NADPH oxidase nox4 provides renoprotection in long-term diabetic nephropathy. J Am Soc Nephrol 2014;25:1237–1254
34. Schägger H. Respiratory chain supercomplexes. IUBMB Life 2001;52:119–128
35. Anand R, Wai T, Baker MJ, et al. The i-AAA protease YME1L and OMA1 cleave OPA1 to balance mitochondrial fusion and fission. J Cell Biol 2014;204:919–929
36. Westermann B. Mitochondrial fusion and fission in cell life and death. Nat Rev Mol Cell Biol 2010;11:872–884
37. Wang W, Wang Y, Long J, et al. Mitochondrial fission triggered by hyperglycemia is mediated by ROCK1 activation in podocytes and endothelial cells. Cell Metab 2012;15:186–200
38. Galloway CA, Yoon Y. Mitochondrial morphology in metabolic diseases. Antioxid Redox Signal 2013;19:415–430
39. Otera H, Wang C, Cleland MM, et al. Mff is an essential factor for mitochondrial recruitment of Drp1 during mitochondrial fission in mammalian cells. J Cell Biol 2010;191:1141–1158
40. Westermann B. Bioenergetic role of mitochondrial fusion and fission. Biochim Biophys Acta 2012;1817:1833–1838
41. Legros F, Lombès A, Frachon P, Rojo M. Mitochondrial fusion in human cells is efficient, requires the inner membrane potential, and is mediated by mitofusins. Mol Biol Cell 2002;13:4343–4354
42. Zanna C, Ghelli A, Porcelli AM, et al. OPA1 mutations associated with dominant optic atrophy impair oxidative phosphorylation and mitochondrial fusion. Brain 2008;131:352–367
43. Cheung EC, Joza N, Steenaart NA, et al. Dissociating the dual roles of apoptosis-inducing factor in maintaining mitochondrial structure and apoptosis. EMBO J 2006;25:4061–4073
44. Brooks C, Wei Q, Cho SG, Dong Z. Regulation of mitochondrial dynamics in acute kidney injury in cell culture and rodent models. J Clin Invest 2009;119:1275–1285

45. Galloway CA, Lee H, Nejjar S, et al. Transgenic control of mitochondrial fission induces mitochondrial uncoupling and relieves diabetic oxidative stress. Diabetes 2012;61:2093–2104
46. Zhan M, Usman IM, Sun L, Kanwar YS. Disruption of renal tubular mitochondrial quality control by Myo-inositol oxygenase in diabetic kidney disease. J Am Soc Nephrol 2015;26:1304–1321
47. Hangen E, Blomgren K, Bénit P, Kroemer G, Modjtahedi N. Life with or without AIF. Trends Biochem Sci 2010;35:278–287
48. Ghezzi D, Sevrioukova I, Invernizzi F, et al. Severe X-linked mitochondrial encephalomyopathy associated with a mutation in apoptosis-inducing factor. Am J Hum Genet 2010;86:639–649
49. Otera H, Ohsakaya S, Nagaura Z, Ishihara N, Mihara K. Export of mitochondrial AIF in response to proapoptotic stimuli depends on processing at the intermembrane space. EMBO J 2005;24:1375–1386
50. Sevrioukova IF. Apoptosis-inducing factor: structure, function, and redox regulation. Antioxid Redox Signal 2011;14:2545–2579